



## Article

# Exploring the Potential of 3D-Printable Agar–Urea Hydrogels as an Efficient Method of Delivering Nitrogen in Agricultural Applications

Wathsala Dissanayake <sup>1</sup>, Hossein Najaf Zadeh <sup>1,2</sup>, Ali Reza Nazmi <sup>1,2</sup>, Campbell Stevens <sup>1</sup>, Tim Huber <sup>3</sup> and Pramuditha L. Abhayawardhana <sup>1,2,\*</sup>

<sup>1</sup> School of Product Design, University of Canterbury, Private Bag 4800, Christchurch 8140, New Zealand; wathsala.dissanayakemudiyanselage@pg.canterbury.ac.nz (W.D.); hossein.najafzadeh@canterbury.ac.nz (H.N.Z.); alireza.nazmi@canterbury.ac.nz (A.R.N.); campbell.stevens@pg.canterbury.ac.nz (C.S.)

<sup>2</sup> Biomolecular Interaction Centre, University of Canterbury, Private Bag 4800, Christchurch 8140, New Zealand

<sup>3</sup> Luxembourg Institute of Science and Technology, 5 Av. des Hauts-Fourneaux, 4362 Luxembourg, Luxembourg; tim.huber@list.lu

\* Correspondence: pram.abhayawardhana@canterbury.ac.nz; Tel.: +64-21467442

**Abstract:** Amidst population growth and challenges with existing fertilizers, the development of smart and environmentally friendly agrochemicals is imperative. While 3D printing is widespread, its potential in slow-release agrochemicals remains unexplored. This proof-of-concept study employed solvent casting and 3D printing to develop agar–urea structures. These structures, comprising 2.5% (*w/w*) agar, incorporated either 7% (*w/w*) or 13% (*w/w*) urea as nitrogen nutrients. Rheological, mechanical, and morphological properties and sorption capabilities were explored. Rheological analysis revealed a substantial impact of urea, enhancing material resistance to deformation. In mechanical tests, inclusion of urea showed no significant impact on compressive strength. SEM analysis confirmed the successful entrapment of urea within the agar matrix. The inclusion of urea resulted in a diminished water sorption capacity, attributed to the urea–water interactions disrupting the hydrogen bonding ability of agar. Agar–urea inks were employed in 3D printing utilizing the direct-ink writing technique, and the nitrogen release behavior was investigated. Results revealed nearly complete urea release in the positive control within 48 h. In contrast, agar–urea formulations with 7% (*w/w*) and 13% (*w/w*) achieved nitrogen release rates of 88.8% and 94.4%, respectively, suggesting potential for 3D-printed agar formulations to modify the immediate release behavior seen in conventional urea fertilizers.

**Keywords:** hydrogel; agar; urea; additive manufacturing; 3D printing; slow-release



**Citation:** Dissanayake, W.; Najaf Zadeh, H.; Nazmi, A.R.; Stevens, C.; Huber, T.; Abhayawardhana, P.L. Exploring the Potential of 3D-Printable Agar–Urea Hydrogels as an Efficient Method of Delivering Nitrogen in Agricultural Applications. *Polysaccharides* **2024**, *5*, 49–66.

<https://doi.org/10.3390/polysaccharides5010004>

Academic Editor: Luminita Marin

Received: 30 January 2024

Revised: 23 February 2024

Accepted: 1 March 2024

Published: 7 March 2024



**Copyright:** © 2024 by the authors. Licensee MDPI, Basel, Switzerland. This article is an open access article distributed under the terms and conditions of the Creative Commons Attribution (CC BY) license (<https://creativecommons.org/licenses/by/4.0/>).

## 1. Introduction

According to estimations, the population of our planet will approach 8.6 billion by 2030, 9.8 billion by 2050, and 11.2 billion by 2100, which forecasts a noticeable increase from the current global population of 8.1 billion people [1]. Synchronically, there will be a pressing need for a 70% expansion in worldwide food production by the year 2050, which will draw attention to the significant demands on sources including land, water, labor, utilities, fuel, and nutrient fertilizers [2]. Nitrogenous fertilizers are chemical fertilizers widely employed to enhance agricultural productivity [3] and urea [CO(NH<sub>2</sub>)<sub>2</sub>] stands out as the foremost nitrogenous fertilizer applied worldwide on account of its rich nitrogen content of 46%. Projections indicate that by 2050, the annual application of urea in agriculture is expected to increase by approximately 130–150 million tons to meet the prevailing agricultural demand [4]. This surge can result in a considerable economic burden, given

the substantial cost of fertilizer, particularly impacting countries primarily reliant on agriculture [5]. Furthermore, it will have serious detrimental effects on the natural ecosystem and the environment [6].

The inefficient nutrient utilization of nitrogenous fertilizers often emerges from conventional fertilizer release rates exceeding the rate at which nutrients are absorbed by plants, or the conversion of nutrients/fertilizers into forms that are not readily usable by crops [7]. Hence, the Nutrient Utilization Efficiency (NUE) of urea is constrained to a range of 30–35%, with a substantial portion of nitrogen escaping from the fertilizer through processes such as volatilization and leaching into the soil and surrounding environment. The latter pathway substantially contributes to eutrophication in aquatic systems, which is specifically an obstacle to the pursuit of reasonable agricultural sustainability [8]. Noticeably, chemical fertilizers identified as a major source of rising N<sub>2</sub>O emissions [9] contribute significantly to stratospheric ozone depletion and pose a dual challenge to global environmental issues [10]. Despite advancements in slow-release fertilizer mechanisms within the 4R nutrient management concept, challenges persist in optimizing nutrient release through these formulations. Elevated costs and detrimental environmental impacts are particularly associated with non-degradable organic/inorganic polymer coating materials [11] and may lead to lasting soil pollution spanning decades or centuries [12]. In anticipation of increased demand for slow-release fertilizers, the European Union (EU) implemented mid-2021 restrictions, primarily addressing the use of microplastics as urea coating materials. From 2026 onwards, only biodegradable materials will be approved for urea slow-release coatings [13].

Within the realm of biodegradable materials, hydrogels stand out as highly promising nutrient carrier substances for transporting fertilizer nutrients, which can be released in a slow manner [14]. Hydrogels are crosslinked three-dimensional network architectures made from an assembly of artificial and/or natural polymers. They are renowned for their remarkable ability to absorb and retain water to a substantial degree [15]. The water-holding capability of a hydrogel is primarily attributed to the prevalence of certain hydrophilic groups in its polymer network particularly carboxyl, hydroxyl, amide, and others [16]. Owing to their well-established biocompatibility, facile synthesis, and broad spectrum of applications, hydrogels have secured a greater degree of attention in recent decades [17]. Specifically, they have demonstrated extensive applications in regenerative medicine [18], in drug delivery [19], in controlled-release devices in agricultural applications [20], as a bio-adsorbent [21], in wound healing [22], in food packaging [23], and in separation systems [24]. In slow-release fertilizer applications, hydrogels demonstrate the ability to release nitrogen in a controlled manner through various mechanisms including diffusion, swelling, and degradation [16]. Their proven properties make them promising candidates for combining with nitrogenous fertilizers, thereby reducing irrigation needs, adverse environmental effects, and fertilizer loss while facilitating the gradual release of nitrogen [25,26]. Recently, super-absorbent hydrogels and synthetic hydrogels have shown significant promise in the market, whereas natural hydrogels have drawn more attention because of their availability, environmental safety, and cost-effectiveness [27,28]. Among these natural hydrogels, chitosan- [29], starch- [3], cellulose- [30], gelatin- [31], and algae-based hydrogels including alginate [32], carrageenan [33], agar [34] and agarose [35] have attracted great research interest towards slow-release fertilizer applications.

In the pool of naturally available hydrogels, agar is a natural polysaccharide-based hydrocolloid seaweed with strong gelling properties [36]. Agar has numerous applications in food [37], drugs [38], beauty products [39], healthcare [40] and biotech industries [41]. Due to its high demand, global agar production increased from 6800 tons in 2002 to 9600 tons in 2009 [42]. A global growth rate of 4.6% is forecast for the next five years [43]. Agar comprises two polysaccharides, namely, the gelling component agarose and the sulfated nongelling component agaropectin. At around 85 °C, agar liquefies in both water and organic solvents and forms a gel upon cooling [44]. It encompasses galacto-pyranose dimers that alternate between galactose and 3,6-anhydro- $\alpha$ -galactopyranose units and are linked by alternating  $\alpha$ -1,3 and  $\beta$ -1,4-linkages [45]. It has the capability to form semi-rigid,

thermo-reversible gels that are hydrophilic by dispersing the powder agar in water, then heating and finally cooling. The final stage involves arranging agar chains into an organized structure, with aggregates of co-axial helices forming the connections of the 3D gel network [46]. Furthermore, agar contains numerous hydroxyl groups that can potentially create intermolecular or intramolecular hydrogen bonds with urea molecules [47]. Numerous studies have discovered that agar can be employed as a matrix for the prolonged release of pharmaceuticals [48–50]. The study conducted by Sampson et al. [34] explored the use of agar as a coating material for soluble NPK fertilizer in both capsular and granular slow-release formulations. In contrast, agar hydrogel is utilized in a double network hydrogel system with starch for herbicide control release, and it has been shown that agar helps promote soil health [51].

3D printing, also known as Additive Manufacturing (AM), is a technique for fabricating engineered structures guided by a 3D model. It involves layer-by-layer assembly of materials using a 3D printer, in contrast to conventional fabrication techniques focused on material removal and shaping [52]. AM generates a complex structured product with excellent accuracy and significantly reduced material waste and contrasts with the limitations of conventional machining, forging, and casting methods [53]. Due to their exceptional properties, hydrogels hold great promise for diverse 3D printing applications [54], including biosensors [55], electronics [56], biomedicine [57], and food packaging [58], and have prominently advanced tissue engineering applications [59]. Notably, hydrogels based on chitosan/alginate have been specifically designed for use as active wound dressings [60]. Furthermore, in response to the increasing demand for personalized food products in recent decades, agar-based hydrogel substances also have garnered popularity in 3D food printing [61]. For instance, agar is combined with gelatin hydrogel in a 3D jet printer to formulate tailored chewable soft meals [62]. Konjac glucomannan is utilized in extrusion-based 3D food printing with agar to upgrade rheological characteristics and smooth the extrusion [63]. Within an agricultural framework, 3D printing has been used to manufacture equipment for irrigation and urban farming practices in recent decades [64]. However, to the best of our knowledge, the application of 3D printing for fabricating customized agricultural formulations with a specific focus on slow release has not yet been comprehensively explored. This study aims to evaluate the potential of agar–urea hydrogel structures for delivering nitrogen nutrients. Through solvent casting and extrusion-based 3D printing, agar–urea structures were developed, and their rheological, mechanical, morphological, sorption capabilities and nitrogen release behavior were assessed.

## 2. Materials and Methods

### 2.1. Materials

Urea (ACS reagent 99.0–100.5%) and agar (high gel strength, plant cell culture tested) powder were purchased from Sigma-Aldrich, St. Louis, MO, USA. Carrageenan powder was purchased from Go Native New Zealand Ltd. (Auckland, New Zealand). Clear and unflavored gelatine powder was purchased from a local supermarket. Agarose powder was purchased from Purolite New Zealand Ltd., Auckland, New Zealand. Washed Sea sand was purchased from a local garden store. Deionized (DI) water was used for all the experiments.

### 2.2. Preparation and Evaluation of Natural Hydrogels for Initial Screening

A preliminary screening study was conducted to identify the most suitable natural hydrogel material for exploring the formulation of 3D-printed slow-release fertilizers. Four naturally occurring hydrogels, namely, carrageenan, gelatin, agarose, and agar, were selected for this purpose. Approximately 50 g of each hydrogel formulation was prepared by adding 1.25 g of hydrogel material into 48.75 g of DI water, resulting in 2.5% (*w/w*) hydrogel formulations. The formulations were subjected to mechanical stirring at 150 rpm using a stirrer at room temperature (RT). The temperature was gradually increased to 95 °C using a hot plate while continuously stirring at 150 rpm to ensure proper dissolution of hydrogel in water. Once a homogeneous hydrogel formulation was achieved, it was

removed from the hot plate and cooled down to 60 °C. Then, 3.50 g and 6.50 g of urea were added into the 2.5% (*w/w*) hydrogel formulation to prepare 2.5% (*w/w*) hydrogel combined with 7% (*w/w*) and 13% (*w/w*) urea, respectively. Temperature was maintained at 60 °C under continuing constant stirring at 200 rpm to ensure thorough dissolution. The prepared formulations consisting of hydrogel, urea, and DI water were cooled down to 40 °C and the solvent cast into pre-prepared cube-shaped molds and allowed to be set for 20 min. Subsequently, the molded formulations with dimensions of  $\sim 10 \times 10 \times 10$  mm were transferred to a refrigerator at 4 °C for 10 min. These formulations were then weighed and stored in labeled air-tight containers until initial screening tests were conducted. These tests, which were aimed at selecting the most suitable natural hydrogel for the intended function, included visual observation for microbial contamination at RT with varying humidity, tolerability tests under various temperatures and humidity, extrudability using five different needle sizes: 22G  $\frac{1}{4}$ ", 22G  $\frac{1}{2}$ ", 25G  $\frac{1}{4}$ ", 25G  $\frac{1}{2}$ ", 27G  $\frac{1}{4}$ ", 27G  $\frac{1}{2}$ ", and water sorption. The water sorption capacity was measured by drying the hydrogel samples at room temperature for 7 days and then placing the dried samples in 200 mL of DI water. After 6 h, they were retrieved from the DI water, and their weights were measured after careful wiping to remove any excess surface water. The water sorption capacity was calculated using the following formula [29]:

$$\text{Water Sorption Capacity} = \frac{(W_s - W_d)}{W_d} \quad (1)$$

where  $W_d$  and  $W_s$  represent the weight of the initial dried sample and swollen sample, respectively.

### 2.3. Solvent Casting of the Agar-Based Hydrogel Formulations

Results of the preliminary screening suggested the suitability of agar for the design of the next experiments. A control formulation of 2.5% *w/w* agar ( $A_{2.5}$ ) and two test formulations: 2.5% *w/w* agar–7% *w/w* urea ( $AU_7$ ) and 2.5% *w/w* agar–13% *w/w* urea ( $AU_{13}$ ) were prepared and solvent cast following the same methodology described above (Section 2.2).

### 2.4. Characterizations of Solvent Cast Agar-Based Hydrogel Formulations

#### 2.4.1. Differential Scanning Calorimetry

A DSC8500 (PerkinElmer, Waltham, MA, USA) Differential Scanning Calorimeter (DSC) was employed to explore the thermal behavior and phase shifts of  $A_{2.5}$  gel samples in order to obtain their gelation and melting temperatures. Approximately 7 mg of agar gel samples was utilized. Tests were conducted across a temperature range spanning 20–105 °C, employing a heating/cooling rate of 20 °C/min. A continuous nitrogen stream flowing at a volume rate of 20 mL/min was supplied during the DSC analysis. To avoid thermal memory effects, the specimens underwent a preliminary thermal cycling procedure involving both heating and cooling phases. Hermetic pans were utilized throughout the study and the pans were sealed after loading with the sample prior to testing.

#### 2.4.2. Rheological Analysis

Rheological measurements were executed directly on the liquid formulations (Section 2.2), using an Anton Paar Modular Compact Rheometer MCR 302 (Anton Paar, Graz, Austria). The employed measurement system consisted of a cone plate (CP50-1), with a Peltier plate serving as the cell. Prior to loading the samples onto the lower plate, the system was heated to 60 °C to avoid solidification of the formulation onto the plate. For each test, a freshly prepared mixture was heated to 60 °C and carefully deposited onto the lower plate. The upper element was then lowered to achieve a gap distance of 0.102 mm, and any excess material was removed. The system temperature was then adjusted to the measurement temperature of 30 °C. The tests were conducted at a low temperature of 30 °C using freshly prepared samples for each test to avoid sample dehydration. To understand the viscoelastic properties of the formulations, amplitude sweeps were conducted on each sample, em-

ploying a fixed frequency of 1 Hz and a strain ranging from 0.0001 to 1%. This allowed for an understanding of the complex moduli and overall flow properties of the formulation, including the storage modulus ( $G'$ ) and loss modulus ( $G''$ ), and the loss factor ( $\tan\delta$ ) in response to applied shear strain.

#### 2.4.3. Mechanical Properties

Compression tests were carried out using an MTS Criterion Model 43 Universal Testing machine (MTS in Eden Prairie, MN, USA) to explore the mechanical properties of the hydrogel samples. All tests were conducted at room temperature using solvent-cast samples with dimensions of  $\sim 10 \times 10 \times 10$  mm. Cylindrical clamps with a diameter of 40 mm were employed. Force application was accomplished with a 0.5 kN load cell, and a consistent crosshead speed of 1 mm/min was maintained. Prior to the testing, excess water on the samples was effectively removed using microfiber wipe paper (Kimberly-Clark, Irving, TX, USA). To prevent dehydration during the compression tests and eliminate the possibility of shear stress between the machine clamp and the part, a thin layer of low-viscosity silicon oil (Silk One drop 3054 silicone lubricant oil, Auckland, New Zealand) was applied. Additionally, the tests and replicates were conducted at room temperature with swift execution to minimize the duration between tests, ensuring minimal exposure of the hydrogel samples to air. A preload of 0.1 N was introduced to the samples positioned between the compression clamps and yield tests were then conducted. The test was conducted in triplicate for each formulation, and the results are reported as the mean value with the standard deviation.

#### 2.4.4. Scanning Electron Microscopy (SEM)

SEM was conducted to explore the morphological characteristics of the A<sub>2.5</sub>, AU<sub>7</sub>, and AU<sub>13</sub> formulations. Hydrogel samples were subjected to freeze-drying for SEM analysis. Rapid freezing was achieved by immersing the hydrogel samples in liquid nitrogen. Subsequently, freeze-drying was conducted at  $-50$  °C for 36 h, utilizing a Labconco freeze dryer (Labconco Corporation, Kansas City, MO, USA). Following the freeze-drying process, hydrogel samples underwent manual fracturing to prepare fracture surfaces suitable for SEM analysis. A carbon coating process was applied in two cycles for 90 s at 25 mA using an Emitech K975X coater (Quorum Technologies Ltd., East Grinstead, UK). Field Emission Scanning Electron Microscopy (FE-SEM) JEOL 7000F FE-SEM (JEOL Ltd., Tokyo, Japan) was employed with a probe current of 10 mA and under an acceleration voltage of 5 kV. Additionally, the pore diameters of all samples were calculated using ImageJ software (Version 1.54, 2023, Wayne Rasband, NIH, Madison, WI, USA).

#### 2.4.5. Water Sorption Capacity

The water sorption capacity of hydrogel samples was assessed using a standard weighing method. The samples were subjected to freeze-drying by immersing in liquid nitrogen followed by freeze-drying at  $-50$  °C for 36 h using a Labconco freeze drier (Labconco Corporation, Kansas City, MO, USA). The freeze-dried and pre-weighed hydrogel samples were then immersed in DI water. At certain time intervals (30, 60, 90, and 120 min), the hydrogel samples were retrieved from DI water and their weights were measured after careful wiping to remove any excess surface water. The experiment was conducted in triplicate for each formulation and the results are reported as the mean value accompanied by the standard deviation. The water sorption capacity was calculated using Equation (1) (Section 2.2).

#### 2.5. Preparation of Agar-Based Hydrogel Formulations for 3D Printing

Approximately 100 g samples of the control A<sub>2.5</sub> and two test formulations; AU<sub>7</sub> and AU<sub>13</sub> were prepared for 3D printing using the same method of formulation just prior to molding as described above (Section 2.2).

### 2.6. Determination of Ideal 3D Printing Parameters

To achieve optimal 3D printing, it was imperative to ascertain the optimal temperature range. Printing at room temperature was deemed ineffective, as the solution would rapidly gelate, leading to the obstruction of the printer nozzle. To overcome this challenge, a temperature-controlled print head was employed, and the gelation temperature of the various formulations was determined. This involved preparing the formulation mixtures as outlined in Section 2.5 and subjecting them to different temperatures, starting at 50 °C and systematically decreasing the temperature. Subsequently, the formulation was hand-extruded onto a small plate using a small syringe to observe the extrusion behavior. The plate was maintained at room temperature throughout the experiment. The optimal temperature range for printing was identified to be between 37 °C and 44 °C. Additionally, it was determined that the formulation mixtures needed approximately 1 h at 37 °C to achieve readiness prior to initiating the 3D printing process. Ambient conditions played a crucial role in influencing the viscosity of the formulation mixture, necessitating temperature adjustments on hotter and cooler days to achieve optimal viscosity.

Furthermore, continuous adjustments to the printing pressure were required during the printing process due to inconsistent temperatures throughout the barrel (printing reservoir). This adjustment was facilitated using the pressure regulator of the Cellink Inkredible + 3D Bioprinter to maintain a constant extrusion rate. Maintaining control over printing parameters and temperature within the specified ideal ranges resulted in more consistent printing behavior, characterized by uniform shape and precision. Consequently, the ideal 3D printing parameters were identified as a temperature range of 37 °C to 44 °C, pressure ~3 kPa, printing head speed of 10 mm/s, and line height of 1 mm.

### 2.7. 3D Printing

After identifying the ideal 3D printing parameters as described in the above Section 2.6, the prepared formulations (Section 2.5) were poured directly into two Cellink barrels (BICO, Gothenburg, Sweden). These barrels were immediately placed in the temperature-controlled holders of the 3D bioprinter and kept for approximately 60 min to equilibrate to the desired temperature. Then, 3D printing was performed using the 18 gauge 32 mm nozzle. During printing, the printing pressure was continuously adjusted to ensure a consistent extrusion rate. After successfully 3D printing cylindrical-shaped A<sub>2.5</sub>, AU<sub>7</sub>, and AU<sub>13</sub> samples with dimensions of ~5 mm radius (r) and ~10 mm height (h), the samples were immediately transferred to individual airtight containers and stored in a refrigerator at 4 °C until characterization.

### 2.8. Nitrogen Release Studies of 3D Printed Agar-Based Hydrogel Formulations

The method for urea slow-release study described by Gungula et al. [65] was adapted and modified for this study. A 250 mL cylindrical, graduated glass separatory funnel was used to test the nitrogen release behavior of the following: 3D printed AU<sub>7</sub>, 3D printed AU<sub>13</sub>, 3D printed A<sub>2.5</sub> (negative control), and conventional urea powder (positive control). Triplicates of each of the above samples were tested. Each separatory funnel was filled with 150 g of washed and autoclaved sea sand. 1 L of DI water was added to the column to wash the sand until clear water was collected. The weighed test or control samples were added to the surface of the sand column covering a central circular area of about one-inch diameter. Approximately 50 g of separately washed sea sand was added to the top of each set-up covering the test/control samples. The weight of the conventional urea powder was calculated based on the amounts of urea estimated in the AU<sub>13</sub> formulation. Approximately 50 mL of DI water was gently introduced to the top surface of the sand column, facilitating the collection of leachates from the soil into 15 mL centrifuge tubes. The same draining procedure was repeated for each sand column with 50 mL of DI water each time at the following time intervals: 12, 24, 48, 72, 96, 120, 144, 168, 264, and 312 h. All collections of leachates were stored in a freezer until the total nitrogen content was analyzed using an Elementar Vario TOC cube (Elementar Analyse Systeme GmbH, Langenselbold,

Germany). Finally, the cumulative nitrogen release % of the AU<sub>7</sub> and AU<sub>13</sub> formulations was calculated and analyzed compared to negative and positive control samples. The cumulative release of nitrogen was calculated as follows [66]:

$$Q_n (\%) = \frac{M_s}{M_t} \times 100\% \quad (2)$$

where  $Q_n$  represents the cumulative nitrogen %,  $M_s$  denotes the accumulated mass of total nitrogen in leachate, and  $M_t$  indicates the mass of total nitrogen content of the formulation, respectively.

### 3. Results and Discussion

#### 3.1. Initial Screening for the Selection of Most Suitable Natural Hydrogel

The visual appearance of hydrogel samples was assessed at room temperature and varying humidity conditions over a 10-day period to identify any physical changes and potential microbial contamination. The observations suggested that carrageenan and agarose hydrogel samples showed a significantly shriveled, dried, and reduced size compared to agar and gelatin hydrogel samples. It was evident that all urea-containing hydrogel samples showed no visible microbial growth compared to the respective non-urea-containing samples. The antimicrobial study conducted by Arafa et al. [67] demonstrated the inhibitory effects of urea-loaded hydrogel formulations on microbial growth. Tolerability tests were conducted at 25 °C with 60% humidity and at 40 °C with 75% humidity over a 10-day period. These tests also confirmed that carrageenan and agarose hydrogel samples displayed a shriveled, dried appearance and were reduced in size compared to agar hydrogel samples when temperature and humidity conditions were increased.

To assess the 3D printability of the hydrogels, extrudability tests were carried out and the results confirmed that all urea-containing samples could easily extrude through the 22G ¼" and the 22G ½". Carrageenan, gelatin, and agar hydrogel samples were able to be extruded through the 22G ¼" needle, but not the agarose hydrogel sample. It was concluded that mainly urea-containing agar and carrageenan hydrogel samples were compatible with varying needle sizes and demonstrated a favorable extrudability capacity, thus confirming their suitability for 3D printing even without any heating.

During water sorption tests, it was noted that agarose and agar hydrogel samples without urea exhibited notably higher sorption capacities compared to their respective counterparts containing urea. This observation suggests that urea molecules may interfere with the hydrogen bonding ability of hydrogels, emphasizing their potential for slow-release applications in agricultural formulations. While agarose and agar samples containing urea demonstrated favorable water sorption behaviors, carrageenan and gelatin samples containing urea exhibited unexpectedly high levels of swelling, making them unsuitable candidates for the intended purpose. Gelatin, a soluble protein compound obtained through partial collagen hydrolysis, can undergo denaturation under certain conditions [68]. Given its frequent use as an additive in protein denaturation, urea is presumed to contribute to gelatin denaturation by interfering with its secondary and tertiary structures. The behavior of carrageenan with urea in water compared to carrageenan alone can be influenced by various factors, including the concentrations of carrageenan and urea, the type of carrageenan, and the specific conditions of the water sorption experiment. Urea could have disrupted the hydrogen bonding network within the carrageenan gel under our experimental conditions. It is important to note that the specific interactions between gelatin or carrageenan and urea can be complex and may vary based on the type of hydrogel (e.g., kappa, iota, lambda carrageenan) and the specific experimental conditions. Experimental studies, such as water sorption tests conducted under controlled conditions, would be needed to provide detailed insights into the unusually high swelling behavior of the two gels with urea.

After assessing the initial results related to microbial contamination tolerance, adaptability to temperature and humidity variations, extrudability capacity, and water sorption

potential, over a tested period, it was concluded that among the tested hydrogels, agar emerged as the most suitable hydrogel material for the subsequent experimental phase. This phase would delve into investigating its solvent casting and 3D printability attributes, physical, rheological, mechanical, and morphological properties, and nitrogen release potential as a matrix for slow-release fertilizer formulation.

### 3.2. Characterizations of Solvent Cast Agar-Based Hydrogel Formulations

#### 3.2.1. Differential Scanning Calorimetry

DSC was performed to determine the melting ( $T_m$ ) and gelation ( $T_g$ ) temperatures of the agar hydrogel ( $A_{2.5}$ ) as illustrated in Figure 1. These values are crucial for identifying the ideal temperature range for mixing agar with urea during 3D printing while shielding against urea decomposition. The  $A_{2.5}$  formulation showed a pronounced endothermic peak at 83.8 °C with a melting enthalpy of 0.44 J/g which represents the melting process of the agar hydrogel. The  $T_m$  of pure agar was reported to be 83.9 °C [69]. The slight variation in  $T_m$  values of pure agar samples is likely attributed to the various seaweed sources/origins and processing conditions of natural agar [70]. This discrepancy has been observed to result in the identification of distinct endothermic peaks in agar gels from diverse sources, occurring at temperature intervals ranging from 75 °C to 90 °C [71].

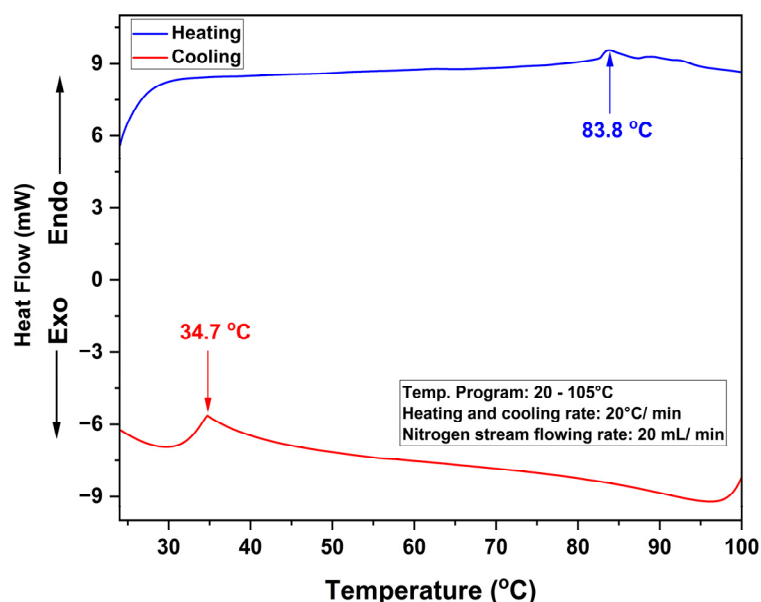


**Figure 1.** DSC thermographs of  $A_{2.5}$  formulation during heating (blue) and cooling (red) trace.

In order to dissolve the agarose fraction in water, heating it to temperatures exceeding 80–90 °C is required to break down the robust interactions among the agarose chains. Following dissolution, it adopts a uniform solution state capable of transitioning into a gel upon cooling below its Upper Critical Solution Temperature (UCST) [72]. This singular exothermic peak observed in the cooling curve is associated with the sol–gel transition of pure agar [73]. When considering the exothermic peak associated with  $A_{2.5}$ , which exhibits a narrower profile compared to the endothermic peak, it becomes apparent at 34.7 °C with an enthalpy change of 2.21 J/g. Pino-Ramos et al. [74] identified  $T_g$  at 33 °C, attributable to the presence of agarose and agaropectin within the agar hydrogel. This observed peak may be ascribed to the gelation process in agarose solutions, which arises from the accumulation of the double helices of agarose, aided by intermolecular bonding of hydrogen atoms and the generation of microcrystalline junction regions [75]. In summary, it is evident that the observed endothermic and exothermic peaks, occurring at 83.8 °C and 34.7 °C, are respectively the establishment and disruption of hydrogen bonds among agar polymer strands, leading to the formation of physical gels and, primarily, the aggregation

or disintegration of the agar double helices. By analyzing the obtained results, it was determined that 60 °C, representing within the range between the obtained  $T_m$  and  $T_g$  of  $A_{2.5}$ , is the ideal temperature for the 3D printing experiments.

### 3.2.2. Rheological Analysis

Amplitude sweeps were employed to elucidate the viscoelastic behavior of hydrogel formulations, with the dependence of viscoelastic moduli ( $G'$  and  $G''$ ) and loss factor ( $\tan\delta$ ) vs. applied shear strain depicted in Figure 2. These strain sweep tests were used to determine the linear viscoelastic (LVE) region and to comprehend how viscoelastic properties are influenced by the incorporation of urea into the agar hydrogel network. The region of constant  $G'$ ,  $G''$  and  $\tan\delta$  defines the LVE range [76]. This region signifies the range in which tests can be conducted without compromising the sample structure. Beyond the critical strain threshold, the gel structure breaks down with  $G'$  decreasing at the end of the LVE region, indicating dependence on the applied strain [77]. A longer LVE region implies greater stability to deformation. All hydrogel formulations, including  $A_{2.5}$ ,  $AU_7$ , and  $AU_{13}$ , exhibit a pronounced dominance of  $G'$  over  $G''$ , confirming the prevalence of elastic characteristics over viscous properties. This observation underscores a robust gel behavior across all formulations.

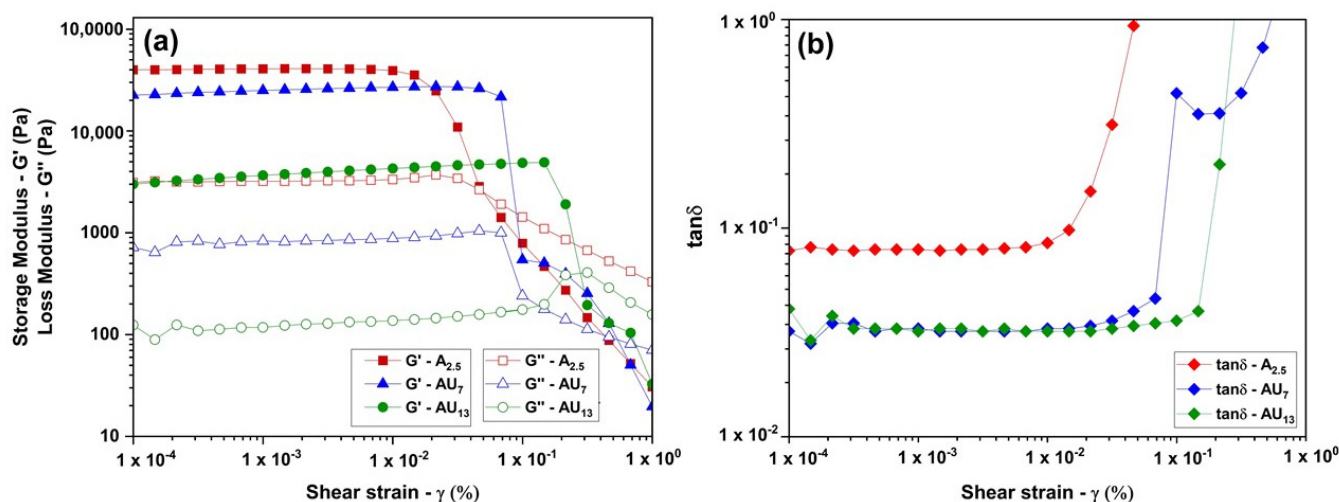


**Figure 2.** (a) Storage modulus ( $G'$ ) and loss modulus ( $G''$ ) graphs and (b)  $\tan\delta$  graphs as a function of shear strain for  $A_{2.5}$ ,  $AU_7$  and  $AU_{13}$  formulations at 30 °C.  $G'$ ,  $G''$ , and  $\tan\delta$  are denoted by filled, unfilled, and diamond shapes, respectively.

The  $A_{2.5}$  formulation displays a higher  $G'$  value at nearly 40 kPa and is closely aligned with the findings of the study by Norziah et al. [78] on 1.5% ( $w/w$ ) agar at 30 °C, and demonstrates a more rigid and denser gel structure of agar hydrogel. This occurrence is likely a result of enhanced molecular aggregation of agar polymer chains, contributing to the formation of a rigid structure. In the case of other samples where agar is mixed with urea, the behavior is slightly different. When compared to the  $A_{2.5}$ , the  $AU_{13}$  formulations exhibit a lower  $G'$  due to the presence of urea, resulting in a more flexible gel structure. The network becomes less rigid with the presence of urea molecules in the agar matrix. The diminished gel strength ( $G'$  and  $G''$ ) in hydrogel formulations with urea ( $AU_7$  and  $AU_{13}$ ) can be attributed to both reduced crosslinking density in their networks and an increased plasticization effect of urea on the network chains. A similar observation was noted in a study by Wei et al. [79] during the synthesis of urea-embedded grafted starch hydrogels. Nevertheless, the  $G'$  value of the  $AU_7$  formulation closely approximates that of the  $A_{2.5}$ .

As depicted in Figure 2, the presence of urea has a notable impact on the extension of the LVE region in  $AU_7$  and  $AU_{13}$  formulations, resulting in a material more resistant to deformation with increasing urea concentration. In the case of the  $A_{2.5}$ , the  $G'$  value

begins to decrease at 0.01% strain, signifying the LVE region between 0.0001% and 0.01%. In contrast, AU<sub>7</sub> and AU<sub>13</sub> samples exhibit longer LVE regions of 0.0001–0.03% and 0.0001–0.14%, respectively, compared to the A<sub>2.5</sub> sample. This phenomenon is likely due to the entrapment of urea, which enhances the gel network's elasticity through the physical entanglement of urea molecules in the agar hydrogel matrix. At strain values of 0.04%, 0.6%, and 0.3%,  $G''$  crosses  $G'$  for the A<sub>2.5</sub>, AU<sub>7</sub>, and AU<sub>13</sub> samples, respectively. This outcome suggests a loss of network strength with increasing strain. Within the two agar-urea formulations, AU<sub>7</sub> manifests a pronounced elastic characteristic in contrast to AU<sub>13</sub>, as indicated by the absence of crossover until reaching a 0.6% strain value. Outside the LVE region, the material's viscous properties become dominant, and it begins to behave like a fluid.

Furthermore, upon examining  $\tan\delta$  ( $G''/G'$ ) values within the LVE range, the substantial difference in  $\tan\delta$  between agar-urea (AU<sub>7</sub> and AU<sub>13</sub>) formulations and the A<sub>2.5</sub> underscores the profound influence of urea on the interactions among agar chains. Typically, the loss factor  $\tan\delta$  serves as an indicator of the dynamic viscoelastic behavior of samples. When  $\tan\delta > 1$ ,  $G''$  dominates, indicating mainly fluid properties, whereas  $\tan\delta < 1$  signifies samples with predominantly elastic properties [63]. Across all our formulations,  $\tan\delta$  remains below 1, indicating their predominantly elastic nature and gel behavior. After analyzing  $\tan\delta$  values within the LVE range, it becomes evident that the inclusion of urea in agar hydrogel formulations leads to a reduction in the loss factor, signifying an enhancement in the strength of the hydrogel network. In the case of AU<sub>7</sub> and AU<sub>13</sub>,  $\tan\delta$  increases with higher urea concentration, indicating a progressively less developed network of hydrogels. A parallel observation was noted in a study on the synthesis of urea-embedded grafted starch hydrogels conducted by Wei et al. [79].

### 3.2.3. Mechanical Properties

The mechanical characteristics of A<sub>2.5</sub>, AU<sub>7</sub>, and AU<sub>13</sub> formulations were assessed through uniaxial compression tests. The samples underwent compression loading until the propagation of cracks resulted in structural failure, allowing for the calculation of compressive strength and Young's modulus. Young's modulus is calculated within the strain range of 0.4% to 13% and compressive strength between 1 kPa and 33 kPa. The formulation exhibits clear rupture damage when the tension approaches the maximum bearing stress, after which the stress swiftly decreases (Figure 3). The maximum compressive strength of the A<sub>2.5</sub> formulation was 92 kPa. Considering that 97.5% ( $w/w$ ) of the formulation is water, the plasticizing effect of water molecules in the agar hydrogel [80] and the physical entanglements of 2.5% ( $w/w$ ) agar polymer chains and intermolecular forces of the polymers contribute to the compressive strength of the 2.5% ( $w/w$ ) agar hydrogel. The inclusion of 7% ( $w/w$ ) urea does not remarkably impact the compressive strength of the agar-urea hydrogel structures. Moreover, an increase in urea content from 7% ( $w/w$ ) to 13% ( $w/w$ ) leads to a slight reduction in the strength of the formulation (refer to Table 1). The higher amount of urea molecule content potentially causes slight denaturation in the agar biopolymer, which could account for the slight compressive strength reduction [81]. Furthermore, at higher urea loading levels, the lack of consistent urea dispersion caused an unequal distribution of stress throughout the agar matrix, hence the reduction in compressive strength. This reduction in compressive strength could also be influenced by the existence of pores, particularly at higher urea loading levels.

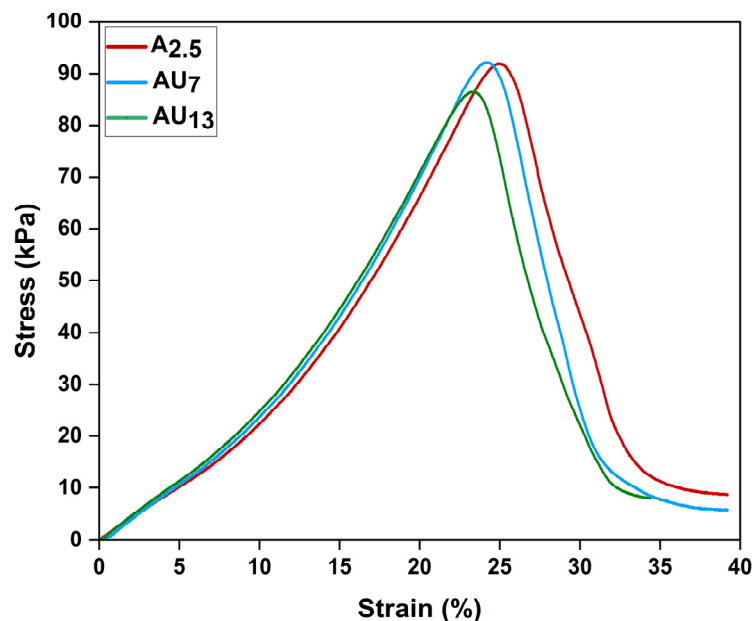


**Figure 3.** Stress–strain curve of A<sub>2.5</sub>, AU<sub>7</sub>, and AU<sub>13</sub> formulations.

**Table 1.** Compressive strength and Young’s modulus of A<sub>2.5</sub>, AU<sub>7</sub>, and AU<sub>13</sub> formulations.

Formulation	Average Compressive Strength (kPa)	Average Young’s Modulus (kPa)
A <sub>2.5</sub>	92.0 ± 6.2	238 ± 10.1
AU <sub>7</sub>	92.2 ± 1.5	256 ± 8.4
AU <sub>13</sub>	86.4 ± 1.3	260 ± 2.5

The Young’s modulus for A<sub>2.5</sub> was 238 kPa, which is a value similar to the Young’s moduli of 2% (*w/v*) pure agar at RT reported by Thompson et al. [73] and 2% (*w/w*) agar reported by Nayar et al. [82]. As Table 1 illustrates, the introduction of urea into the agar matrix shows slightly higher Young’s modulus values, though statistically not significant, imparting gradually enhanced stiffness and making the agar formulation slightly stiffer.

### 3.2.4. SEM Morphology

SEM was performed to study the morphological surface characterization of A<sub>2.5</sub>, AU<sub>7</sub>, and AU<sub>13</sub> urea formulations (Figure 4) using freeze-dried samples. According to the SEM image of A<sub>2.5</sub> (Figure 4a), it exhibited a uniform, regular porous structure and a slightly smooth surface when compared to agar–urea surface morphology behavior. Interestingly, it represents a well-known porous, three-dimensional structure that encompasses the assembly of agar spherical networks [83]. However, the addition of urea molecules steadily enhanced the surface roughness of the A<sub>2.5</sub> formulation. When analyzing the average pore size, initially A<sub>2.5</sub> showed pores with dimensions of 148 ± 26 nm, followed by AU<sub>7</sub> and AU<sub>13</sub> exhibiting average diameter values of 90 ± 19 nm and 153 ± 32 nm, respectively. This pore size distribution confirmed that the porosity of AU<sub>7</sub> was moderately reduced and consisted of urea crystals that guaranteed urea entrapment, as shown in Figure 4b, which would then have an impact on the porous structure of the network as well as nutrient release behavior [67]. Conversely, after incorporating urea into the hydrogel matrix, a porous structure can still be observed in the hydrogel (as shown in Figure 4b,c). This suggests that urea molecules are not interacting or bonding with the hydrogel via any covalent/hydrogen bonds, as the urea entrapment occurred within the porous matrix of the hydrogel.

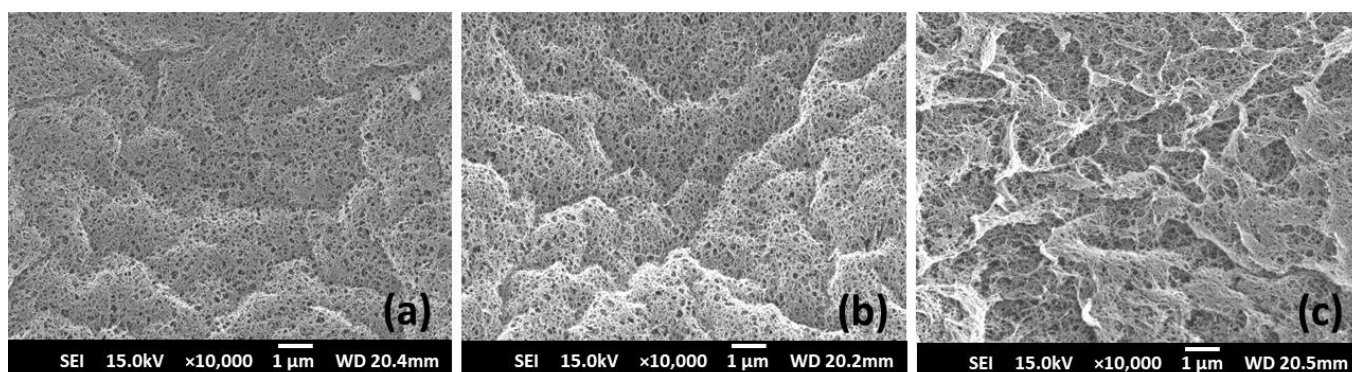


**Figure 4.** SEM images of (a)  $A_{2.5}$  (b)  $AU_7$  and (c)  $AU_{13}$  formulations (scale bar: 1  $\mu\text{m}$ , magnification:  $\times 10,000$ , voltage: 15.0 kV).

Comparatively, the  $AU_7$  formulation showed a slightly rough nature and porous surface (Figure 4b) compared to the  $AU_{13}$  formulation (Figure 4c), indicating the homogenous trapping of urea inside the hydrogel network. However, few lumps and a less homogeneous nature were seen on its rough surface when the urea concentration was raised to 13%. When the urea concentration was raised from 7% to 13%, some crystallized urea particles were recognized on the irregular porous structure of agar with no uniformities; this phenomenon may be due to the precipitation of saturated urea. Similar morphological observations due to the precipitation of saturated urea were reported by Wei et al. [79] when the urea loading rate increased from 40% to 60% within a starch hydrogel matrix. Conclusively, the urea concentration in hydrogel may affect how the urea is dispersed within the agar hydrogel matrix, which may have a significant effect on the slow-release ability and water permeability properties of the synthesized agricultural formulations.

### 3.2.5. Water Sorption Capacity

The water sorption capacity was investigated using freeze-dried agar-based hydrogel compositions (Table 2), initially focusing on  $A_{2.5}$  and then also exploring the influence of urea addition with  $AU_7$  and  $AU_{13}$  formulations. The results, as illustrated in Table 2, indicate the water sorption behavior of the respective compositions over different time intervals. It is observed that the water sorption capacity increased significantly after 120 min compared to 30 min. This finding is consistent with the well-established property of hydrogels, which possess a high capacity to absorb water owing to the abundance of hydrophilic groups within their structure. This phenomenon underscores the potential of hydrogels for slow-release fertilizer applications, where controlled water absorption and retention over time are essential for providing gradual nutrient release to plants.

**Table 2.** Water sorption capacities of  $A_{2.5}$ ,  $AU_7$ , and  $AU_{13}$  formulations at 30, 60, 90, and 120 min time intervals.

Formulation	Average Capacity ( $\Delta\text{g}/\text{g}_{\text{initial}}$ )			
	30 min	60 min	90 min	120 min
$A_{2.5}$	$17.82 \pm 2.10$	$18.30 \pm 1.68$	$18.28 \pm 1.55$	$18.77 \pm 1.62$
$AU_7$	$6.52 \pm 0.04$	$6.61 \pm 0.10$	$6.58 \pm 0.33$	$6.71 \pm 0.13$
$AU_{13}$	$3.61 \pm 0.05$	$3.58 \pm 0.08$	$3.77 \pm 0.02$	$3.76 \pm 0.11$

$A_{2.5}$  exhibited notably higher water sorption capacity across all time intervals (30, 60, 90, and 120 min) compared to  $AU_7$  and  $AU_{13}$ . The higher water sorption capacity of the agar formulation ( $A_{2.5}$ ) aligns with the well-documented hydrophilic nature of agar, stemming from its abundant hydroxyl groups capable of forming hydrogen bonds with water molecules [84]. Agar hydrogel shows more hydrophilicity as the agaropectin

present in agar hydrogel comprises a heterogeneous collection of smaller branching and sulfated molecules [85]. Moreover, agar is a sulfated polysaccharide, and unlike other polysaccharides, its charged group allows its chains to be more elongated and boosted in water-attracting capabilities [86]. Consequently, A<sub>2.5</sub> demonstrated a superior capacity for water absorption and retention, underscoring the pivotal role of agar in determining water sorption capabilities.

For further analysis of the A<sub>2.5</sub>, AU<sub>7</sub>, and AU<sub>13</sub> formulations, the average water sorption capacity after 120 min was explored. The influence of urea addition on agar hydrogel was another critical aspect of this study. The introduction of urea into the agar matrix resulted in a significant reduction in water sorption capacity. This decline became more pronounced as urea concentrations increased from 0% (A<sub>2.5</sub>) to 7% (AU<sub>7</sub>) and 13% (AU<sub>13</sub>). Specifically, AU<sub>7</sub> exhibited a diminished water sorption capacity of approximately 6.71  $\Delta g/g_{\text{initial}}$  compared to the agar-only counterpart (A<sub>2.5</sub>). Similar trends were observed in the third formulation of AU<sub>13</sub>. AU<sub>13</sub> demonstrated the lowest water sorption capacity among the tested samples, measuring only about 3.76  $\Delta g/g_{\text{initial}}$ .

The sorption capacity of AU<sub>7</sub> and AU<sub>13</sub> steadily reduced, feasibly due to the dissolution of non-crosslinked urea and polymer molecules. Additionally, this decline could be attributed to the hydrolysis of the hydrogel structure [29]. Furthermore, this reduction could be attributed to the presence of urea while interacting with water molecules, which lack the extensive hydrogen bonding capabilities of agar. Consequently, urea disrupts the hydrogen bonding network within the agar matrix, leading to a diminished capacity to retain water. Analyzing the data over varying time intervals revealed minor fluctuations in water sorption capacity. While these variations were not substantial, they indicated a slight time-dependent aspect to water sorption in agar-based hydrogels. Water sorption capacity tended to marginally increase with longer exposure times, although the overall trends associated with agar concentration and urea addition remained consistent. These findings have significant implications for potential applications of agar-based hydrogels, particularly in scenarios where controlled water sorption is crucial, such as in smart and slow-release applications in agriculture. The capability to customize agar–urea formulations facilitates the attainment of distinct water sorption characteristics, aligning with the needs of various industries.

### 3.3. Nitrogen Release Studies of 3D Printed Agar-Based Hydrogel Formulations in Soil Medium

Figure 5 illustrates the cumulative release rates of the positive control (conventional urea powder), AU<sub>7</sub>, and AU<sub>13</sub> in soil medium. The results demonstrated that conventional urea powder released its nitrogen at a quicker pace than other formulations due to its high solubility. Within 72 h, 99% of the urea of the positive control had been released into the soil, which is consistent with previously reported urea release characterizations in a soil medium by Gungula et al. [65]. Typically, within the soil environment, a minor fraction of urea undergoes hydrolysis; the majority, decomposed by microorganisms, transforms into ammonia gas, resulting in urea loss within a few days [87]. In the context of agar–urea hydrogel formulations, both AU<sub>7</sub> and AU<sub>13</sub> formulations demonstrated a gradual and cumulative release of nitrogen nutrients when compared to the positive control, mainly from 24–48 h to around 72 h (Figure 5). This observation affirms the viability of our agar–urea formulations. Evidently, the capability of absorbing a higher amount of water within the hydrogel matrix might be substantially accountable for the improvement in the gradual-release feature of the prepared agar–urea formulations [88]. The cumulative release rates of the formulations after 12 h were 13.6%, 85.4%, 39.0%, and 45.3% for the negative control (A<sub>2.5</sub>), positive control, AU<sub>7</sub>, and AU<sub>13</sub> respectively. In the experimental setup, the soil itself was subjected to autoclaving. Nevertheless, throughout the study, the presence of any residual microbes in the soil could have led to the generation of nitrogen-containing compounds. The interactions or contaminations of nitrogen-containing compounds in the soil medium might be responsible for the slight amounts of nitrogen released from the negative control. In the agar–urea formulations, the weakly entrapped/bonded urea on

the exterior surface of the agar hydrogel caused them to swiftly diffuse or dissolve into the solution, which may have affected the rapid release within the first 12 h. Then, agar-urea formulations exhibited slow nitrogen release behavior from 24 h to around 48–72 h. According to the hydrogel-urea study conducted by Song et al. [87], urea molecules were embedded as small molecules in the swelled hydrogel when the soil and water-retentive hydrogel were blended. Due to the concentration gradient between the water-absorbing material and the surrounding soil, nitrogen release achieves a consistent state. Despite that, AU<sub>13</sub> exhibited a speedy release pattern when compared to AU<sub>7</sub>. The cumulative nitrogen release percentage of AU<sub>7</sub> was 39%, 70%, 88.8%, 96.3%, and 99.1% after 12, 24, 48, 72, and 96 h, respectively, which indicates that in AU<sub>7</sub>, the hydrogel had certain slow-release characteristics, making it suitable to be considered for a potential nutrient carrier in agricultural formulations. In contrast, AU<sub>13</sub> emerged with quicker cumulative nitrogen release rates of 45.3%, 82.3%, 94.4%, 98.5%, and 99.6% at the same time intervals indicated above. Interestingly, our morphological analysis shows a consistent relationship with release data, and in accordance with the SEM images, the AU<sub>13</sub> formulation encountered a crystal structure of urea, revealing the precipitation of saturated urea crystals in the hydrogel substrate. Therefore, out of the two test formulations, the AU<sub>7</sub> formulation can be considered the optimum formulation for slow-release fertilizer applications. Optimization of these formulations through architecture and 3D printing parameters should be aimed at achieving a reliable prolonged release pattern over an extended period of time.

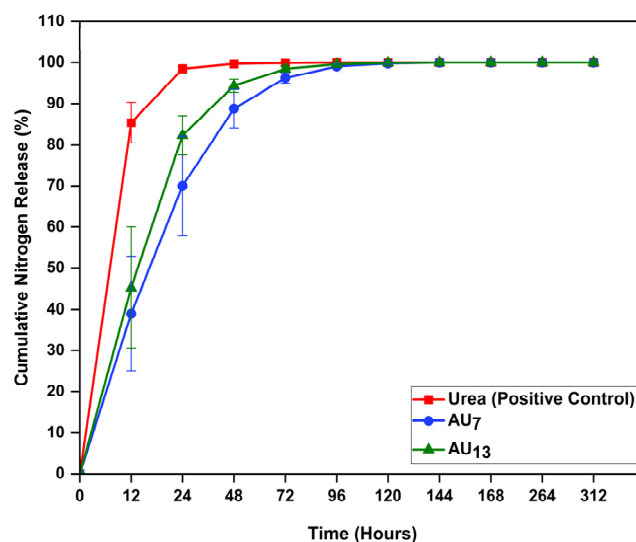


**Figure 5.** Cumulative nitrogen release % of urea powder (positive control), AU<sub>7</sub>, and AU<sub>13</sub> formulations in soil medium.

#### 4. Conclusions

Agar hydrogel was blended with urea in two different weight ratios to formulate a slow-release agricultural formulation. The agar-urea inks underwent solvent casting, and their rheological, mechanical, morphological, and water sorption capabilities were systematically analyzed. Rheological results unveiled the impact of urea on extending the LVE region. Incorporating urea did not yield a significant impact on the mechanical properties. SEM characterization confirmed the successful entrapment of urea molecules in the porous agar hydrogel matrix. The AU<sub>7</sub> and AU<sub>13</sub> formulations exhibited diminished water sorption capacities, compared to A<sub>2.5</sub>. Simultaneously, an extrusion-based 3D printing technique was employed to fabricate agar-urea hydrogel formulations, and their nitrogen release behavior was assessed. After approximately 72 h, the cumulative nitrogen release rates were 99.9%, 96.3%, and 98.5% for urea powder (positive control), AU<sub>7</sub>, and AU<sub>13</sub>, respectively. The findings of this proof-of-concept study underscore the promise of 3D-printable agar-urea hydrogel structures, necessitating further exploration

as slow-release agricultural formulations. Moving forward, the next phase of the project will focus on optimizing 3D printing parameters and refining the architectural design of structures to enhance formulation efficiency, cost-effectiveness, and scalability, all of which are critical factors for the practical implications of the outcomes.

**Author Contributions:** Methodology/formal analysis/investigation, W.D., P.L.A., A.R.N., H.N.Z. and C.S.; writing—original draft preparation, W.D., P.L.A., A.R.N. and H.N.Z.; writing—review, editing, and supervision, P.L.A., A.R.N., H.N.Z. and T.H.; funding acquisition, P.L.A. All authors have read and agreed to the published version of the manuscript.

**Funding:** Funding was provided to P. Abhayawardhana by BIC Seed Funding (reference code: 41700:5009:417SEED:0:1) from Biomolecular Interaction Centre, University of Canterbury and by the UC Early Career Research Accelerator Fund 2022 (grant code: 23-09161) from University of Canterbury. W. Dissanayake is a recipient of a PhD Scholarship funded by the School of Product Design, University of Canterbury, Christchurch, New Zealand (reference code: ECRAF2309161).

**Institutional Review Board Statement:** Not applicable.

**Data Availability Statement:** The data presented in this study are available in the article.

**Acknowledgments:** The authors would like to express their gratitude to the funding sources mentioned above as well as Gemma Thompson and Min Min for their contributions associated with the preliminary stages of the study. Additionally, the authors acknowledge D. Holland for sharing his expertise to help advance the project.

**Conflicts of Interest:** The authors declare no conflict of interest.

## References

1. Okolie, C.C.; Danso-Abbeam, G.; Groupson-Paul, O.; Ogundeji, A.A. Climate-Smart Agriculture Amidst Climate Change to Enhance Agricultural Production: A Bibliometric Analysis. *Land* **2023**, *12*, 50. [[CrossRef](#)]
2. Kottegoda, N.; Sandaruwan, C.; Priyadarshana, G.; Siriwardhana, A.; Rathnayake, U.A.; Berugoda Arachchige, D.M.; Kumarasinghe, A.R.; Dahanayake, D.; Karunaratne, V.; Amaratunga, G.A. Urea-Hydroxyapatite Nanohybrids for Slow Release of Nitrogen. *ACS Nano* **2017**, *11*, 1214–1221. [[CrossRef](#)]
3. Xiao, X.; Yu, L.; Xie, F.; Bao, X.; Liu, H.; Ji, Z.; Chen, L. One-step method to prepare starch-based superabsorbent polymer for slow release of fertilizer. *Chem. Eng. J.* **2017**, *309*, 607–616. [[CrossRef](#)]
4. Tapia-Hernández, J.A.; Madera-Santana, T.J.; Rodríguez-Félix, F.; Barreras-Urbina, C.G. Controlled and Prolonged Release Systems of Urea from Micro-and Nanomaterials as an Alternative for Developing a Sustainable Agriculture: A Review. *J. Nanomater.* **2022**, *2022*, 5697803. [[CrossRef](#)]
5. Vejan, P.; Khadiran, T.; Abdullah, R.; Ahmad, N. Controlled release fertilizer: A review on developments, applications and potential in agriculture. *J. Control. Release* **2021**, *339*, 168–3659. [[CrossRef](#)]
6. Wang, X. Managing Land Carrying Capacity: Key to Achieving Sustainable Production Systems for Food Security. *Land* **2022**, *11*, 484. [[CrossRef](#)]
7. Zulfiqar, F.; Navarro, M.; Ashraf, M.; Akram, A.; Munné-Bosch, S. Nanofertilizer use for sustainable agriculture: Advantages and limitations. *Plant Sci.* **2019**, *289*, 110270. [[CrossRef](#)]
8. Latha, M.; Subramanian, K.S.; Sharmila, D.J.S.; Raja, K.; Rajkishore, S.K.; Chitdeshwari, T. Urea-Lignin/Chitosan Nanocomposite as Slow-Release Nanofertilizer. *ACS Agric. Sci. Technol.* **2023**, *3*, 463–476. [[CrossRef](#)]
9. Zhang, Y.; Wang, W.; Yao, H. Urea-based nitrogen fertilization in agriculture: A key source of N<sub>2</sub>O emissions and recent development in mitigating strategies. *Arch. Agron. Soil Sci.* **2022**, *69*, 663–678. [[CrossRef](#)]
10. Hayashi, K.; Itsubo, N. Damage factors of stratospheric ozone depletion on human health impact with the addition of nitrous oxide as the largest contributor in the 2000s. *Int. J. Life Cycle.* **2023**, *28*, 990–1002. [[CrossRef](#)]
11. Dhiman, S.; Yadav, A.; Debnath, N.; Das, S. Application of Core/Shell Nanoparticles in Smart Farming: A Paradigm Shift for Making the Agriculture Sector More Sustainable. *J. Agric. Food Chem.* **2021**, *69*, 3267–3283. [[CrossRef](#)]
12. Chen, F.; Miao, C.; Duan, Q.; Jiang, S.; Liu, H.; Ma, L.; Li, Z.; Bao, X.; Lan, B.; Chen, L.; et al. Developing slow release fertilizer through in-situ radiation-synthesis of urea-embedded starch-based hydrogels. *Ind. Crops Prod.* **2023**, *1159*, 19171. [[CrossRef](#)]
13. Kavitha, R.; Latifah, O.; Ahmed, O.H.; Charles, P.W.; Susilawati, K. Potential of Rejected Sago Starch as a Coating Material for Urea Encapsulation. *Polymers* **2023**, *15*, 1863. [[CrossRef](#)] [[PubMed](#)]
14. Pushpamalar, J.; Langford, S.J.; Ahmad, M.B.; Lim, Y.Y.; Hashim, K. Eco-friendly smart hydrogels for soil conditioning and sustain release fertilizer. *Int. J. Environ. Sci. Technol.* **2018**, *15*, 2059–2074. [[CrossRef](#)]
15. Catoira, M.C.; Fusaro, L.; Di Francesco, D.; Ramella, M.; Boccafoschi, F. Overview of natural hydrogels for regenerative medicine applications. *J. Mater. Sci. Mater. Med.* **2019**, *30*, 115. [[CrossRef](#)] [[PubMed](#)]

16. Kaur, P.; Agrawal, R.; Pfeffer, F.M.; Williams, R.; Bohidar, H.B. Hydrogels in Agriculture: Prospects and Challenges. *J. Polym. Environ.* **2023**, *31*, 3701–3718. [[CrossRef](#)]
17. Qu, B.; Luo, Y. Chitosan-based hydrogel beads: Preparations, modifications and applications in food and agriculture sectors—A review. *Int. J. Biol. Macromol.* **2020**, *152*, 437–448. [[CrossRef](#)] [[PubMed](#)]
18. Chaudhary, S.; Chakraborty, E. Hydrogel based tissue engineering and its future applications in personalized disease modeling and regenerative therapy. *Beni. Suef. Univ. J. Basic. Appl. Sci.* **2022**, *11*, 3. [[CrossRef](#)]
19. Sun, Z.; Song, C.; Wang, C.; Hu, Y.; Wu, J. Hydrogel-Based Controlled Drug Delivery for Cancer Treatment: A Review. *Mol. Pharm.* **2020**, *17*, 373–391. [[CrossRef](#)]
20. Rudzinski, W.E.; Dave, A.M.; Vaishnav, U.H.; Kumbar, S.G.; Kulkarni, A.R.; Aminabhavi, T.M. Hydrogels as controlled release devices in agriculture. *Des. Monomers Polym.* **2002**, *5*, 39–65. [[CrossRef](#)]
21. Xiang, Z.; Tang, N.; Jin, X.; Gao, W. Fabrications and applications of hemicellulose-based bio-adsorbents. *Carbohydr. Polym.* **1189**, 2022, 27845. [[CrossRef](#)] [[PubMed](#)]
22. Liang, Y.; He, J.; Guo, B. Functional Hydrogels as Wound Dressing to Enhance Wound Healing. *ACS Nano* **2021**, *15*, 12687–12722. [[CrossRef](#)] [[PubMed](#)]
23. Panda, P.K.; Sadeghi, K.; Seo, J. Recent advances in poly (vinyl alcohol)/natural polymer based films for food packaging applications: A review. *Food Packag. Shelf Life* **2022**, *33*, 100904. [[CrossRef](#)]
24. Lv, Y.; Xi, X.; Dai, L.; Tong, S.; Chen, Z. Hydrogel as a Superwetting Surface Design Material for Oil/Water Separation: A Review. *Adv. Mater. Interfaces* **2002**, 2021, 8030. [[CrossRef](#)]
25. Singh, N.; Agarwal, S.; Jain, A.; Khan, S. 3-Dimensional cross linked hydrophilic polymeric network ‘hydrogels’: An agriculture boom. *Agric. Water Manag.* **2021**, *253*, 106939. [[CrossRef](#)]
26. Guilherme, M.R.; Aouada, F.A.; Fajardo, A.R.; Martins, A.F.; Paulino, A.T.; Davi, M.F.; Rubira, A.F.; Muniz, E.C. Superabsorbent hydrogels based on polysaccharides for application in agriculture as soil conditioner and nutrient carrier: A review. *Eur. Polym. J.* **2015**, *72*, 365–385. [[CrossRef](#)]
27. Sahmat, S.S.; Rafii, M.Y.; Oladosu, Y.; Jusoh, M.; Hakimian, M.; Mohidin, H. A Systematic Review of the Potential of a Dynamic Hydrogel as a Substrate for Sustainable Agriculture. *Horticulturae* **2022**, *8*, 1026. [[CrossRef](#)]
28. Patra, S.K.; Poddar, R.; Brestic, M.; Acharjee, P.U.; Bhattacharya, P.; Sengupta, S.; Pal, P.; Bam, N.; Biswas, B.; Berek, V.; et al. Prospects of Hydrogels in Agriculture for Enhancing Crop and Water Productivity under Water Deficit Condition. *Int. J. Polym. Sci.* **2022**, 2022, 4914836. [[CrossRef](#)]
29. Vo, P.T.; Nguyen, H.T.; Trinh, H.T.; Nguyen, V.M.; Le, A.-T.; Tran, H.Q.; Nguyen, T.T.T. The nitrogen slow-release fertilizer based on urea incorporating chitosan and poly(vinyl alcohol) blend. *Environ. Technol. Innov.* **2021**, *22*, 101528. [[CrossRef](#)]
30. Pang, L.; Gao, Z.; Feng, H.; Wang, S.; Wang, Q. Cellulose based materials for controlled release formulations of agrochemicals: A review of modifications and applications. *J. Control. Release* **2019**, *316*, 105–115. [[CrossRef](#)] [[PubMed](#)]
31. Yuan, W.; Li, S.; Guan, H.; Zhang, S.; Zhang, Y.; Zhang, M.; Yu, Y.; Chen, X. Preparation and Properties of a Novel Biodegradable Composite Hydrogel Derived from Gelatin/Chitosan and Polylactic Acid as Slow-Release N Fertilizer. *Polymers* **2023**, *15*, 997. [[CrossRef](#)]
32. Shen, Y.; Wang, H.; Li, W.; Liu, Z.; Liu, Y.; Wei, H.; Li, J. Synthesis and characterization of double-network hydrogels based on sodium alginate and halloysite for slow release fertilizers. *Int. J. Biol. Macromol.* **2020**, *164*, 557–565. [[CrossRef](#)] [[PubMed](#)]
33. Li, J.; Zhu, Y.; Liu, M.; Liu, Z.; Zhou, T.; Liu, Y.; Cheng, D. Network interpenetrating slow-release nitrogen fertilizer based on carrageenan and urea: A new low-cost water and fertilizer regulation carrier. *Int. J. Biol. Macromol.* **2023**, *242*, 124858. [[CrossRef](#)] [[PubMed](#)]
34. Sampson, T.; Oguebue, C.; Okpokwasili, G. Production and Application of Agar-based Slow-release Fertilizers, in the Bioremediation of Petroleum Hydrocarbon-impacted Soil. *Br. Biotechnol. J.* **2016**, *13*, 1–13. [[CrossRef](#)]
35. Lin, J.; Jiao, G.; Kermanshahi-Pour, A. Algal Polysaccharides-Based Hydrogels: Extraction, Synthesis, Characterization, and Applications. *Mar. Drugs* **2022**, *20*, 306. [[CrossRef](#)] [[PubMed](#)]
36. Pandya, Y.; Bakshi, M.; Sharma, A.; Pandya, Y.H.; Pandya, H. Agar-agar extraction, structural properties and applications: A review. *Pharma Innov. J.* **2022**, *11*, 1151–1157.
37. Cebrián-Lloret, V.; Martínez-Abad, A.; López-Rubio, A.; Martínez-Sanz, M. Exploring alternative red seaweed species for the production of agar-based hydrogels for food applications. *Food Hydrocoll.* **2024**, *146*, 109177. [[CrossRef](#)]
38. Yin, Z.C.; Wang, Y.L.; Wang, K. A pH-responsive composite hydrogel beads based on agar and alginate for oral drug delivery. *J. Drug Deliv. Sci. Technol.* **2018**, *43*, 12–18. [[CrossRef](#)]
39. Smulek, W.; Grzabka-Zasadzińska, A.; Kilian, A.; Ciesielczyk, F.; Borysiak, S.; Baranowska, H.M.; Walkowiak, K.; Kaczorek, E.; Jarzębski, M. Design of vitamin-loaded emulsions in agar hydrogel matrix dispersed with plant surfactants. *Food Biosci.* **2023**, *53*, 102559. [[CrossRef](#)]
40. Baek, J.S.; Carlomagno, C.; Muthukumar, T.; Kim, D.; Park, J.H.; Song, J.E.; Migliaresi, C.; Motta, A.; Reis, R.L.; Khang, G. Evaluation of Cartilage Regeneration in Gellan Gum/agar Blended Hydrogel with Improved Injectability. *Macromol. Res.* **2019**, *27*, 558–564. [[CrossRef](#)]
41. Lee, W.K.; Lim, Y.Y.; Ho, C.L. Gracilaria as the major source of agar for food, health and biotechnology applications. In *Sustainable Global Resources of Seaweeds Volume 2: Food, Pharmaceutical and Health Applications*; Springer International Publishing: Cham, Switzerland, 2022; Volume 2, pp. 145–161. [[CrossRef](#)]

42. Lee, W.K.; Lim, Y.Y.; Leow, A.T.C.; Namasivayam, P.; Abdullah, J.O.; Ho, C.L. Biosynthesis of agar in red seaweeds: A review. *Carbohydr. Polym.* **2017**, *164*, 23–30. [[CrossRef](#)] [[PubMed](#)]
43. Global Agar-Agar Industry Research Report 2023, Competitive Landscape, Market Size, Regional Status and Prospect. Available online: <https://www.researchreportsworld.com/global-agar-agar-industry-research-report-2023-competitive-landscape-market-22378959> (accessed on 25 January 2024).
44. Khan, M.J.; Guo, Q.; Varley, R. Facile one pot synthesis of strong epoxy/agar hybrid hydrogels. *J. Polym. Res.* **2019**, *26*, 291. [[CrossRef](#)]
45. Duman, O.; Polat, T.G.; Diker, C.Ö.; Tunç, S. Agar/ $\kappa$ -carrageenan composite hydrogel adsorbent for the removal of Methylene Blue from water. *Int. J. Biol. Macromol.* **2020**, *160*, 823–835. [[CrossRef](#)]
46. Sansonetti, A.; Bertasa, M.; Canevali, C.; Rabbolini, A.; Anzani, M.; Scalarone, D. A review in using agar gels for cleaning art surfaces. *J. Cult. Herit.* **2020**, *44*, 285–296. [[CrossRef](#)]
47. Li, W.; Wu, Z.; Zhao, J.; Jiang, M.; Yuan, L.; Guo, Y.; Li, S.; Hu, L.; Xie, X.; Zhang, Y.; et al. Fabrication of dual physically cross-linked polyvinyl alcohol/agar hydrogels with mechanical stability and antibacterial activity for wound healing. *Int. J. Biol. Macromol.* **2023**, *247*, 125652. [[CrossRef](#)]
48. Sadreiarhami, Z.; Morshed, M.; Varshosaz, J. Production and evaluation of polyblend of agar and polyacrylonitrile nanofibers for in vitro release of methotrexate in cancer therapy. *Fibers Polym.* **2015**, *16*, 254–262. [[CrossRef](#)]
49. Date, P.; Ootoor, D. pH Dependent Controlled Release of CTAB Incorporated Dipyrindamole Drug from Agar-Based Hydrogel. *Polym. Plast. Technol. Eng.* **2016**, *55*, 403–413. [[CrossRef](#)]
50. Olak, T.; Turan, A.; Alpaslan, D.; Dudu, T.E.; Aktaş, N. Developing poly(Agar-co-Glycerol-co-Thyme Oil) based organo-hydrogels for the controlled drug release applications. *J. Drug Deliv. Sci. Technol.* **2020**, *60*, 102088. [[CrossRef](#)]
51. Singh, B.; Sharma, D.K.; Negi, S.; Dhiman, A. Synthesis and characterization of agar-starch based hydrogels for slow herbicide delivery applications. *Int. J. Plast. Technol.* **2015**, *19*, 263–274. [[CrossRef](#)]
52. Pérez-Pérez, M.P.; Gómez, E.; Sebastián, M.A. Delphi prospection on additive manufacturing in 2030: Implications for education and employment in Spain. *Materials* **2018**, *11*, 1500. [[CrossRef](#)]
53. Javaid, M.; Haleem, A.; Singh, R.P.; Suman, R.; Rab, S. Role of additive manufacturing applications towards environmental sustainability. *Adv. Ind. Eng. Polym. Res.* **2021**, *4*, 312–322. [[CrossRef](#)]
54. Kaliaraj, G.S.; Shanmugam, D.K.; Dasan, A.; Mosas, K.K.A. Hydrogels—A Promising Materials for 3D Printing Technology. *Gels* **2023**, *9*, 260. [[CrossRef](#)]
55. Distler, T.; Boccaccini, A.R. 3D printing of electrically conductive hydrogels for tissue engineering and biosensors—A review. *Acta Biomater.* **2020**, *101*, 1–13. [[CrossRef](#)] [[PubMed](#)]
56. Yang, R.; Chen, X.; Zheng, Y.; Chen, K.; Zeng, W.; Wu, X. Recent advances in the 3D printing of electrically conductive hydrogels for flexible electronics. *J. Mater. Chem. C Mater.* **2022**, *10*, 5380–5399. [[CrossRef](#)]
57. Rajabi, M.; McConnell, M.; Cabral, J.; Ali, M.A. Chitosan hydrogels in 3D printing for biomedical applications. *Carbohydr. Polym.* **2021**, *260*, 117768. [[CrossRef](#)]
58. Liu, S.; Chen, X.; Zhang, Y. Hydrogels and hydrogel composites for 3D and 4D printing applications. In *3D and 4D Printing of Polymer Nanocomposite Materials: Processes, Applications, and Challenges*; Elsevier: Amsterdam, The Netherlands, 2020; pp. 427–465. [[CrossRef](#)]
59. Gomez-Florit, M.; Pardo, A.; Domingues, R.M.A.; Graça, A.L.; Babo, P.S.; Reis, R.L.; Gomes, M.E. Natural-Based Hydrogels for Tissue Engineering Applications. *Molecules* **2020**, *25*, 5858. [[CrossRef](#)] [[PubMed](#)]
60. Bergonzi, C.; Bianchera, A.; Remaggi, G.; Ossiprandi, M.C.; Bettini, R.; Elviri, L. 3D Printed Chitosan/Alginate Hydrogels for the Controlled Release of Silver Sulfadiazine in Wound Healing Applications: Design, Characterization and Antimicrobial Activity. *Micromachines* **2023**, *14*, 137. [[CrossRef](#)]
61. Mandal, S.; Nagi, G.K.; Corcoran, A.A.; Agrawal, R.; Dubey, M.; Hunt, R.W. Algal polysaccharides for 3D printing: A review. *Carbohydr. Polym.* **2023**, *300*, 120267. [[CrossRef](#)]
62. Serizawa, R.; Shitara, M.; Gong, J.; Makino, M.; Kabir, M.H.; Furukawa, H. 3D jet printer of edible gels for food creation. In Proceedings of the Behavior and Mechanics of Multifunctional Materials and Composites, San Diego, CA, USA, 9–13 March 2014; 2014; 9058, pp. 80–85. [[CrossRef](#)]
63. Rahman, J.M.H.; Shiblee, M.N.I.; Ahmed, K.; Khosla, A.; Kawakami, M.; Furukawa, H. Rheological and mechanical properties of edible gel materials for 3D food printing technology. *Heliyon* **2020**, *6*, e05859. [[CrossRef](#)]
64. Crisostomo, J.L.B.; Dizon, J.R.C. 3D Printing Applications in Agriculture, Food Processing, and Environmental Protection and Monitoring. *Adv. Sustain. Sci. Eng. Technol.* **2021**, *3*, 0210201. [[CrossRef](#)]
65. Gungula, D.T.; Andrew, F.P.; Joseph, J.; Kareem, S.A.; Barminas, J.T.; Adebayo, E.F.; Saddiq, A.M.; Tame, V.T.; Dere, I.; Ahinda, W.J.; et al. Formulation and characterization of water retention and slow-release urea fertilizer based on Borassus aethiopicum starch and Maesopsis eminii hydrogels. *Results Mater.* **2021**, *12*, 100223. [[CrossRef](#)]
66. Wang, K.; Hou, J.; Zhang, S.; Hu, W.; Yi, G.; Chen, W.; Cheng, L.; Zhang, Q. Preparation of a new biochar-based microbial fertilizer: Nutrient release patterns and synergistic mechanisms to improve soil fertility. *Sci. Total Environ.* **2023**, *860*, 160478. [[CrossRef](#)]
67. Arafa, E.G.; Sabaa, M.W.; Mohamed, R.R.; Kamel, E.M.; Elzanaty, A.M.; Mahmoud, A.M.; Abdel-Gawad, O.F. Eco-friendly and biodegradable sodium alginate/quaternized chitosan hydrogel for controlled release of urea and its antimicrobial activity. *Carbohydr. Polym.* **2022**, *291*, 119555. [[CrossRef](#)] [[PubMed](#)]

68. Gomez-Guillen, M.C.; Gimenez, B.; Lopez-Caballero, M.E.; Montero, M.P. Functional and bioactive properties of collagen and gelatin from alternative sources: A review. *Food Hydrocoll.* **2011**, *25*, 1813–1827. [CrossRef]
69. Atef, M.; Rezaei, M.; Behrooz, R. Preparation and characterization agar-based nanocomposite film reinforced by nanocrystalline cellulose. *Int. J. Biol. Macromol.* **2014**, *70*, 537–544. [CrossRef] [PubMed]
70. Prasad, K.; Siddhanta, A.K.; Rakshit, A.K.; Bhattacharya, A.; Ghosh, P.K. On the properties of agar gel containing ionic and non-ionic surfactants. *Int. J. Biol. Macromol.* **2005**, *35*, 135–144. [CrossRef] [PubMed]
71. Suzuki, H.; Sawai, Y.; Takada, M. The Effect of Apparent Molecular Weight and Components of Agar on Gel Formation. *Food Sci. Technol. Res.* **2001**, *7*, 280–284. [CrossRef]
72. Graham, S.; Marina, P.F.; Blencowe, A. Thermoresponsive polysaccharides and their thermoreversible physical hydrogel networks. *Carbohydr. Polym.* **2019**, *207*, 143–159. [CrossRef]
73. Thompson, B.R.; Horozov, T.S.; Stoyanov, S.D.; Paunov, V.N. An ultra melt-resistant hydrogel from food grade carbohydrates. *RSC Adv.* **2017**, *7*, 45535–45544. [CrossRef]
74. Pino-Ramos, V.H.; Duarte-Peña, L.; Bucio, E. Highly crosslinked agar/acrylic acid hydrogels with antimicrobial properties. *Gels* **2021**, *7*, 183. [CrossRef]
75. Fernández, E.; López, D.; Mijangos, C.; Duskova-Smrckova, M.; Ilavsky, M.; Dusek, K. Rheological and thermal properties of agarose aqueous solutions and hydrogels. *J. Polym. Sci. B Polym. Phys.* **2008**, *46*, 322–328. [CrossRef]
76. Cofelice, M.; Messia, M.C.; Marconi, E.; Cuomo, F.; Lopez, F. Effect of the xanthan gum on the rheological properties of alginate hydrogels. *Food Hydrocoll.* **2023**, *142*, 108768. [CrossRef]
77. Ramin, M.A.; Latxague, L.; Sindhu, K.R.; Chassande, O.; Barthélémy, P. Low molecular weight hydrogels derived from urea based-bolaamphiphiles as new injectable biomaterials. *Biomaterials* **2017**, *145*, 72–80. [CrossRef]
78. Norziah, M.H.; Foo, S.L.; Karim, A.A. Rheological studies on mixtures of agar (*Gracilaria changii*) and  $\kappa$ -carrageenan. *Food Hydrocoll.* **2006**, *20*, 204–217. [CrossRef]
79. Wei, X.; Bao, X.; Yu, L.; Liu, H.; Lu, K.; Chen, L.; Bai, L.; Zhou, X.; Li, Z.; Li, W. Correlation Between Gel Strength of Starch-Based Hydrogel and Slow Release Behavior of Its Embedded Urea. *J. Polym. Env.* **2020**, *28*, 863–870. [CrossRef]
80. Yu, H.; Yu, J.; Zhan, M. Study on mechanical behaviour of agar gel in compression mode. *Bulg. Chem. Commun.* **2018**, *1*, 225.
81. Shamsuri, A.A.; Daik, R. Utilization of an ionic liquid/urea mixture as a physical coupling agent for agarose/talc composite films. *Materials* **2013**, *6*, 682–698. [CrossRef] [PubMed]
82. Nayar, V.T.; Weiland, J.D.; Nelson, C.S.; Hodge, A.M. Elastic and viscoelastic characterization of agar. *J. Mech. Behav. Biomed. Mater.* **2012**, *7*, 60–68. [CrossRef]
83. Giordano, A.; Caruso, M.R.; Lazzara, G. New tool for sustainable treatments: Agar spray—Research and practice. *Herit. Sci.* **2022**, *10*, 123. [CrossRef]
84. Zhang, L.; Xiao, Q.; Xiao, Z.; Zhang, Y.; Weng, H.; Chen, F.; Xiao, A. Hydrophobic modified agar: Structural characterization and application in encapsulation and release of curcumin. *Carbohydr. Polym.* **2023**, *308*, 120644. [CrossRef]
85. Bao, X.; Hayashi, K.; Li, Y.; Teramoto, A.; Abe, K. Novel agarose and agar fibers: Fabrication and characterization. *Mater. Lett.* **2010**, *64*, 2435–2437. [CrossRef]
86. Jumaidin, R.; Sapuan, S.M.; Jawaid, M.; Ishak, M.R. Effect of agar on physical properties of thermoplastic starch derived from sugar palm tree. *Pertanika J. Sci. Technol.* **2017**, *25*, 1235–1248. Available online: <https://www.researchgate.net/publication/326253661> (accessed on 11 September 2023).
87. Song, J.; Chen, L.; Niu, Y.; Ruan, H. Sustained urea release performance of humic acid hydrogel for green vegetable growth environment evaluation. *J. Porous Mater.* **2022**, *29*, 1747–1758. [CrossRef]
88. Dong, G.; Mu, Z.; Liu, D.; Shang, L.; Zhang, W.; Gao, Y.; Zhao, M.; Zhang, X.; Chen, S.; Wei, M. Starch phosphate carbamate hydrogel based slow-release urea formulation with good water retentivity. *Int. J. Biol. Macromol.* **2021**, *190*, 189–197. [CrossRef] [PubMed]

**Disclaimer/Publisher’s Note:** The statements, opinions and data contained in all publications are solely those of the individual author(s) and contributor(s) and not of MDPI and/or the editor(s). MDPI and/or the editor(s) disclaim responsibility for any injury to people or property resulting from any ideas, methods, instructions or products referred to in the content.